UVicSPACE: Research & Learning Repository

University of Victoria

Faculty of Engineering

Faculty Publications

Interband transition enhanced third harmonic generation from nanoplasmonic gold

Ghazal Hajisalem, Dennis K. Hore, and Reuven Gordon

September 2015

This article was originally published at:

http://dx.doi.org/10.1364/OME.5.002217

Citation for this paper:

Hajisalem, G., Hore, D.K. & Gordon, R. (2015). Interband transition enhanced third harmonic generation from nanoplasmonic gold. *Optical Materials Express*, 5(10), 2217-2224.

Interband transition enhanced third harmonic generation from nanoplasmonic gold

Ghazal Hajisalem,[1] Dennis K. Hore,[2] and Reuven Gordon[1,*]

[1]*Department of Electrical and Computer Engineering, University of Victoria, Victoria, BC, V8P 5C2, Canada*
[2]*Department of Chemistry, University of Victoria, Victoria, BC, V8W 3V6, Canada*
[*]*rgordon@uvic.ca*

Abstract: We measure third harmonic generation (THG) as a function of infrared fundamental wavelength for gold nanoparticles over a gold film. An order of magnitude enhancement in THG is found at ~2.5 eV. We ensure that this enhancement is away from plasmonic resonances, so that it may be attributed directly to the ultrafast third-order susceptibility of gold. Using a simple relation between linear and third-order susceptibilities in conjunction with the linear response of gold, we show that the experimental results agree well with the enhancement from interband transitions. This result is interesting for potential applications leveraging telecom-band sources, such as third harmonic deep-tissue imaging with plasmonic nanoparticle markers.

©2015 Optical Society of America

OCIS codes: (250.5403) Plasmonics; (310.6628) Subwavelength structures, nanostructures; (160.4330) Nonlinear optical materials.

References and links

1. S. Kim, J. Jin, Y.-J. Kim, I.-Y. Park, Y. Kim, and S.-W. Kim, "High-harmonic generation by resonant plasmon field enhancement," Nature **453**(7196), 757–760 (2008).
2. N. J. Halas, S. Lal, W.-S. Chang, S. Link, and P. Nordlander, "Plasmons in strongly coupled metallic nanostructures," Chem. Rev. **111**(6), 3913–3961 (2011).
3. W. L. Barnes, A. Dereux, and T. W. Ebbesen, "Surface plasmon subwavelength optics," Nature **424**(6950), 824–830 (2003).
4. E. Prodan, C. Radloff, N. J. Halas, and P. Nordlander, "A hybridization model for the plasmon response of complex nanostructures," Science **302**(5644), 419–422 (2003).
5. K. F. MacDonald, Z. L. Sámson, M. I. Stockman, and N. I. Zheludev, "Ultrafast active plasmonics," Nat. Photonics **3**(1), 55–58 (2009).
6. N. Large, M. Abb, J. Aizpurua, and O. L. Muskens, "Photoconductively loaded plasmonic nanoantenna as building block for ultracompact optical switches," Nano Lett. **10**(5), 1741–1746 (2010).
7. T. Xu, X. Jiao, and S. Blair, "Third-harmonic generation from arrays of sub-wavelength metal apertures," Opt. Express **17**(26), 23582–23588 (2009).
8. M. Airola, Y. Liu, and S. Blair, "Second-harmonic generation from an array of sub-wavelength metal apertures," J. Opt. A, Pure Appl. Opt. **7**(2), S118–S123 (2005).
9. A. Nahata, R. A. Linke, T. Ishi, and K. Ohashi, "Enhanced nonlinear optical conversion from a periodically nanostructured metal film," Opt. Lett. **28**(6), 423–425 (2003).
10. Y. Zhang, N. K. Grady, C. Ayala-Orozco, and N. J. Halas, "Three-dimensional nanostructures as highly efficient generators of second harmonic light," Nano Lett. **11**(12), 5519–5523 (2011).
11. H. Aouani, M. Navarro-Cia, M. Rahmani, T. P. H. Sidiropoulos, M. Hong, R. F. Oulton, and S. A. Maier, "Multiresonant broadband optical antennas as efficient tunable nanosources of second harmonic light," Nano Lett. **12**(9), 4997–5002 (2012).
12. G. Hajisalem, A. Ahmed, Y. Pang, and R. Gordon, "Plasmon hybridization for enhanced nonlinear optical response," Opt. Express **20**(28), 29923–29930 (2012).
13. P. N. Melentiev, A. E. Afanasiev, A. A. Kuzin, A. S. Baturin, and V. I. Balykin, "Subwavelength light localization based on optical nonlinearity and light polarization," Opt. Lett. **38**(13), 2274–2276 (2013).
14. P. N. Melentiev, T. V. Konstantinova, A. E. Afanasiev, A. A. Kuzin, A. S. Baturin, A. V. Tausenev, A. V. Konyaschenko, and V. I. Balykin, "Single nano-hole as a new effective nonlinear element for third-harmonic generation," Laser Phys. Lett. **10**(7), 075901 (2013).
15. P. N. Melentiev, A. E. Afanasiev, A. A. Kuzin, A. S. Baturin, and V. I. Balykin, "Giant optical nonlinearity of a single plasmonic nanostructure," Opt. Express **21**(12), 13896–13905 (2013).

#242926 Received 16 Jun 2015; revised 31 Aug 2015; accepted 8 Sep 2015; published 15 Sep 2015

16. P. N. Melentiev, A. E. Afanasiev, A. A. Kuzin, A. V. Zablotskiy, and V. I. Balykin, "Giant enhancement of two photon induced luminescence in metal nanostructure," Opt. Express **23**(9), 11444–11452 (2015).
17. A. Fiore, V. Berger, E. Rosencher, P. Bravetti, and J. Nagle, "Phase matching using an isotropic nonlinear optical material," Nature **391**(6666), 463–466 (1998).
18. C. G. Durfee III, A. R. Rundquist, S. Backus, C. Herne, M. M. Murnane, and H. C. Kapteyn, "Phase matching of high-order harmonics in hollow waveguides," Phys. Rev. Lett. **83**(11), 2187–2190 (1999).
19. R. H. Stolen and H. W. K. Tom, "Self-organized phase-matched harmonic generation in optical fibers," Opt. Lett. **12**(8), 585–587 (1987).
20. J. Bravo-Abad, A. Rodriguez, P. Bermel, S. G. Johnson, J. D. Joannopoulos, and M. Soljačić, "Enhanced nonlinear optics in photonic-crystal microcavities," Opt. Express **15**(24), 16161–16176 (2007).
21. R. W. Boyd, *Nonlinear Optics*. (Academic Press, 1992).
22. S. Palomba and L. Novotny, "Near-field imaging with a localized nonlinear light source," Nano Lett. **9**(11), 3801–3804 (2009).
23. N. J. Durr, T. Larson, D. K. Smith, B. A. Korgel, K. Sokolov, and A. Ben-Yakar, "Two-photon luminescence imaging of cancer cells using molecularly targeted gold nanorods," Nano Lett. **7**(4), 941–945 (2007).
24. E. J. Sánchez, L. Novotny, and X. S. Xie, "Near-field fluorescence microscopy based on two-photon excitation with metal tips," Phys. Rev. Lett. **82**(20), 4014–4017 (1999).
25. J. T. Krug II, E. J. Sánchez, and X. S. Xie, "Fluorescence quenching in tip-enhanced nonlinear optical microscopy," Appl. Phys. Lett. **86**(23), 233102 (2005).
26. F. Helmchen and W. Denk, "Deep tissue two-photon microscopy," Nat. Methods **2**(12), 932–940 (2005).
27. D. Débarre, W. Supatto, A.-M. Pena, A. Fabre, T. Tordjmann, L. Combettes, M.-C. Schanne-Klein, and E. Beaurepaire, "Imaging lipid bodies in cells and tissues using third-harmonic generation microscopy," Nat. Methods **3**(1), 47–53 (2006).
28. F. Hache, D. Ricard, C. Flytzanis, and U. Kreibig, "The optical Kerr effect in small metal particles and metal colloids: The case of gold," Appl. Phys., A Mater. Sci. Process. **47**(4), 347–357 (1988).
29. C. Sun, F. Vallée, L. H. Acioli, E. P. Ippen, and J. G. Fujimoto, "Femtosecond-tunable measurement of electron thermalization in gold," Phys. Rev. B Condens. Matter **50**(20), 15337–15348 (1994).
30. P. G. Etchegoin, E. C. Le Ru, and M. Meyer, "An analytic model for the optical properties of gold," J. Chem. Phys. **125**(16), 164705 (2006).
31. R. W. Boyd, Z. Shi, and I. De Leon, "The third-order nonlinear optical susceptibility of gold," Opt. Commun. **326**, 74–79 (2014).
32. M. R. Beversluis, A. Bouhelier, and L. Novotny, "Continuum generation from single gold nanostructures through near-field mediated intraband transitions," Phys. Rev. B **68**(11), 115433 (2003).
33. L. A. Gómez and C. B. de Araújo, "Nonlinear optical measurement of gold nanoparticles using the z-scan," Annals of Optics (2006).
34. S. Palomba, M. Danckwerts, and L. Novotny, "Nonlinear plasmonics with gold nanoparticle antennas," J. Opt. A, Pure Appl. Opt. **11**(11), 114030 (2009).
35. G. Hajisalem, M. S. Nezami, and R. Gordon, "Probing the quantum tunneling limit of plasmonic enhancement by third harmonic generation," Nano Lett. **14**(11), 6651–6654 (2014).
36. H. Harutyunyan, G. Volpe, R. Quidant, and L. Novotny, "Enhancing the nonlinear optical response using multifrequency gold-nanowire antennas," Phys. Rev. Lett. **108**(21), 217403 (2012).
37. B. Metzger, M. Hentschel, M. Lippitz, and H. Giessen, "Third-harmonic spectroscopy and modeling of the nonlinear response of plasmonic nanoantennas," Opt. Lett. **37**(22), 4741–4743 (2012).
38. H. Aouani, M. Rahmani, M. Navarro-Cía, and S. A. Maier, "Third-harmonic-upconversion enhancement from a single semiconductor nanoparticle coupled to a plasmonic antenna," Nat. Nanotechnol. **9**(4), 290–294 (2014).
39. B. Metzger, M. Hentschel, T. Schumacher, M. Lippitz, X. Ye, C. B. Murray, B. Knabe, K. Buse, and H. Giessen, "Doubling the efficiency of third harmonic generation by positioning ITO nanocrystals into the hot-spot of plasmonic gap-antennas," Nano Lett. **14**(5), 2867–2872 (2014).
40. D. D. Smith, Y. Yoon, R. W. Boyd, J. K. Campbell, L. A. Baker, R. M. Crooks, and M. George, "Z-scan measurement of the nonlinear absorption of a thin gold film," J. Appl. Phys. **86**(11), 6200–6205 (1999).
41. E. Xenogiannopoulou, P. Aloukos, S. Couris, E. Kaminska, A. Piotrowska, and E. Dynowska, "Third-order nonlinear optical properties of thin sputtered gold films," Opt. Commun. **275**(1), 217–222 (2007).
42. P. Wang, Y. Lu, L. Tang, J. Zhang, H. Ming, J. Xie, F. H. Ho, H. H. Chang, H. Y. Lin, and D. P. Tsai, "Surface-enhanced optical nonlinearty of a gold film," Opt. Commun. **229**(1), 425–429 (2004).
43. M. Lippitz, M. A. van Dijk, and M. Orrit, "Third-harmonic generation from single gold nanoparticles," Nano Lett. **5**(4), 799–802 (2005).
44. A. Marini, M. Conforti, G. Della Valle, H. W. Lee, T. X. Tran, W. Chang, M. A. Schmidt, S. Longhi, P. S. J. Russell, and F. Biancalana, "Ultrafast nonlinear dynamics of surface plasmon polaritons in gold nanowires due to the intrinsic nonlinearity of metals," New J. Phys. **15**(1), 013033 (2013).
45. M. Conforti and G. Della Valle, "Derivation of third-order nonlinear susceptibility of thin metal films as a delayed optical response," Phys. Rev. B **85**(24), 245423 (2012).
46. V. Knittel, M. P. Fischer, T. de Roo, S. Mecking, A. Leitenstorfer, and D. Brida, "Nonlinear photoluminescence spectrum of single gold nanostructures," ACS Nano **9**(1), 894–900 (2015).
47. B. Metzger, L. Gui, and H. Giessen, "Ultrabroadband chirped pulse second-harmonic spectroscopy: measuring the frequency-dependent second-order response of different metal films," Opt. Lett. **39**(18), 5293–5296 (2014).

#242926 Received 16 Jun 2015; revised 31 Aug 2015; accepted 8 Sep 2015; published 15 Sep 2015

48. B. Metzger, L. Gui, J. Fuchs, D. Floess, M. Hentschel, and H. Giessen, "Strong enhancement of second harmonic emission by plasmonic resonances at the second harmonic wavelength," Nano Lett. **15**(6), 3917–3922 (2015).
49. G. Hajisalem, Q. Min, R. Gelfand, and R. Gordon, "Effect of surface roughness on self-assembled monolayer plasmonic ruler in nonlocal regime," Opt. Express **22**(8), 9604–9610 (2014).
50. P. B. Johnson and R. W. Christy, "Optical constants of the noble metals," Phys. Rev. B **6**(12), 4370–4379 (1972).
51. S. Linic, U. Aslam, C. Boerigter, and M. Morabito, "Photochemical transformations on plasmonic metal nanoparticles," Nat. Mater. **14**(6), 567–576 (2015).
52. S. Link and M. A. El-Sayed, "Spectral properties and relaxation dynamics of surface plasmon electronic oscillations in gold and silver nanodots and nanorods," J. Phys. Chem. B **103**(40), 8410–8426 (1999).
53. A. Manjavacas, J. G. Liu, V. Kulkarni, and P. Nordlander, "Plasmon-induced hot carriers in metallic nanoparticles," ACS Nano **8**(8), 7630–7638 (2014).
54. N. Del Fatti, C. Voisin, M. Achermann, S. Tzortzakis, D. Christofilos, and F. Vallée, "Nonequilibrium electron dynamics in noble metals," Phys. Rev. B **61**(24), 16956–16966 (2000).
55. D. Greszik, H. Yang, T. Dreier, and C. Schulz, "Measurement of water film thickness by laser-induced fluorescence and Raman imaging," Appl. Phys. B **102**(1), 123–132 (2011).
56. J. Aizpurua, G. W. Bryant, L. J. Richter, F. J. García de Abajo, B. K. Kelley, and T. Mallouk, "Optical properties of coupled metallic nanorods for field-enhanced spectroscopy," Phys. Rev. B **71**(23), 235420 (2005).

1. Introduction

Nonlinear plasmonics brings the functionality of nonlinear optics, including wavelength conversion and switching, to the nanoscale [1–6]. The goal is to obtain efficient light energy conversion or optical functionality at the subwavelength scale [7–16]. This is in contrast to conventional nonlinear optics, which typically requires phase matching over long distances or microcavities to obtain high conversion efficiency [17–21]. Ohmic losses present a challenge for nonlinear plasmonics; however, there are still applications where near-field generation is of interest even with losses (e.g., nonlinear imaging [22,23], near-field scanning optical microscopy [24, 25]). In particular, deep tissue imaging can be enhanced by using an IR fundamental wavelength along with second harmonic generation (SHG) [26] or THG [27] that is less susceptible to scattering.

Gold is a promising nonlinear plasmonic material because it has relatively low losses along with a large nonlinear susceptibility, with $\chi^{(3)}$ ranging from 10^{-19} to 10^{-14} m^2/V^2 [28–31], depending upon the physical mechanism of the nonlinearity and corresponding timescale of interest. With gold, it is possible to focus the light down to the nanoscale to enhance the nonlinear response [32–35]. Recent works have focused on THG from gold nanoantennas, showing substantial enhancement from optimized antenna structures [36–39].

For fast nonlinear processes (at the picosecond to subpicosecond scale), the interband transition in gold can provide three orders of magnitude larger $\chi^{(3)}$ than for off-resonance wavelengths [31,40,41]. Past works exploring the nonlinear response focused on fundamental wavelengths resonant with the interband transition between the 5d and 6s-6p bands [40–42]. This requires incident wavelengths around 500 nm and emitted wavelengths at a third of this value (in the UV) for THG. A few works have reported on THG using ~1550 nm sources, which is approximately a third of the interband transition energy and therefore close to the resonance condition [14,15,35,43]. Figure 1 shows schematically the three photon resonant processes for this wavelength range [21,32]. This is a relevant wavelength range because of the connection to low-loss fiber-optic technology; for example, leveraging erbium-doped fiber amplifier based laser sources. It is important to distinguish the nearly instantaneous response required for THG from $\chi^{(3)}$ enhancements that come from processes longer than the carrier thermalization, since those slower processes do not yield THG [29,44,45]. Three-photon photoluminescence is also a distinct process from THG since it involves carrier relaxation [32,46].

#242926 Received 16 Jun 2015; revised 31 Aug 2015; accepted 8 Sep 2015; published 15 Sep 2015
(C) 2015 OSA

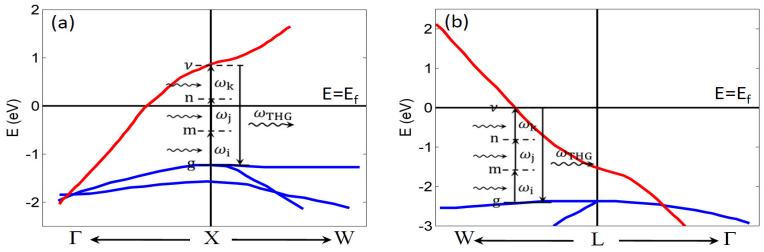

Fig. 1. Band structure near the (a) X and (b) L points of the Brillouin zone of gold (adapted from Refs. 21 and 32). The blue curves are the 5d bands, and the red curve is the 6s-6p band. The black line at $E = E_f = 0$ is the Fermi level. Resonant contribution to the third-order susceptibility is shown for ~2-3 eV energies.

Recently, we probed the quantum tunneling limits of THG using a 100 fs 1570 nm source and obtained THG that could saturate the imaging CCD at only 40 ms acquisition time for the sample with optimized spacer layer thickness [35]. Intrigued by the large signal, here we investigate the wavelength dependence of the THG for the same system using a 22 ps pulse width laser to determine if interband transitions are playing a role in the strong response, and to map out the dispersion of this response (i.e., to resolve spectrally the interband contributions). Also, we use an analytic model for the dielectric function of gold in which contributions of the interband transitions are considered [21,30]. This model agrees well with our experimental observations. It should be mentioned that this work is analogous to recent investigations of SHG of metals near the interband transition [47,48]; however, the third harmonic process is distinct for many reasons (including selection rules). Compared to femtosecond works, the picosecond pulses used here provide narrow spectral resolution.

2. Experimental setup

Figure 2(a) shows a schematic of the gold nanoparticles over ultraflat gold film sample. The sample was prepared following the same method as in our previous work, selecting the gap spacing with highest THG [35]. This sample was chosen primarily for three reasons: 1) there was a good uniformity of nonlinear response due to the uniform gap size; 2) the plasmon resonance was away from the THG and fundamental wavelengths to separate interband enhancement from plasmonic enhancement; and, 3) the ultraflat substrate minimizes THG that arises from uncontrolled surface roughness. Briefly, an ultraflat gold film was prepared by evaporating 30 nm of gold onto silicon wafer at a rate of 1 Å/s and temperature of 200 °C. Promptly, the gold film was coated with a thin layer of optical epoxy (Norland Optical Adhesive 61) followed by a clean glass slide. The epoxy was cured by UV light for 5 min. The gold film was "stripped" from the silicon wafer, revealing the ultraflat surface of gold film. The ultraflat film, with average root mean squared roughness of 0.06 nm [49], was used to minimize the nonlinear contribution from surface roughness. To fabricate a self-assembled monolayer (SAM) of 3-amino-1-propanethiol hydrochloride (739294, Sigma-Aldrich) on the fresh ultraflat gold film, 1 mM solution of the alkanethiol was prepared in ethanol. A SAM layer was formed by immersing the ultraflat substrate into the alkanethiol solution for 18 h, followed by sonication for 2 min and rinsing with ethanol for 15 s. The process of sonication and rinsing was repeated four times. Finally, the substrate was dried using nitrogen gas. 60 nm diameter gold nanoparticles (BBI) were immobilized electrostatically on top of the SAM by incubating the substrate with 500 µL of the colloidal stock for 30 min followed by rinsing with deionized water (USF Elga, Maxima, model Scientific MK3, 18.2 MΩ-cm) for 15 s and drying with a steam of nitrogen gas. Figure 2(b) shows a scanning electron microscopy image of a typical sample that confirms a uniform distribution of gold nanoparticles over the film. This image was taken from a high density area of nanoparticles near the edge of the sample,

#242926 Received 16 Jun 2015; revised 31 Aug 2015; accepted 8 Sep 2015; published 15 Sep 2015
(C) 2015 OSA

which accumulate due to the drying process. The region where optical measurements were made had a nanoparticle density of 30 ± 5 per 100 microns squared, as confirmed by scanning electron microscope characterization.

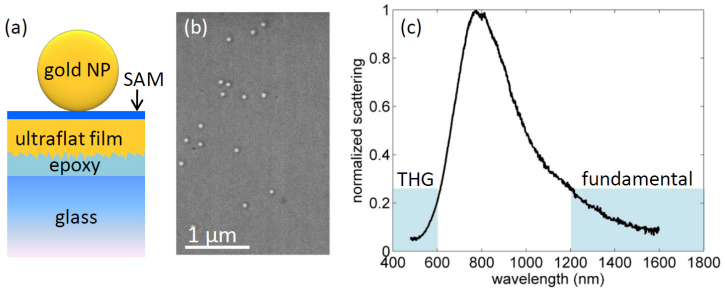

Fig. 2. (a) A schematic of gold nanoparticle (NP) separated from ultraflat gold film by a SAM. (b) Scanning electron microscope image of a typical sample. (c) Dark field scattering spectrum of the sample does not show resonance in the fundamental region as well as the THG region (within the limits of our detection system).

The linear optical properties of the sample were studied by taking the dark field scattering spectrum, using the same method as our previous work [35]. However, the setup was modified to cover both visible and near-IR regions; here the scattered beam from the sample was directed to a visible spectrometer (QE65000, Ocean Optics) and a near-IR spectrometer (NIR-512, Ocean Optics) using a bifurcated fiber (QBIF400-VIS-NIR, Ocean Optics). The normalized spectrum, for each region, was obtained by subtracting the spectrum of a blank ultraflat film from the sample's spectrum and dividing it by the white light source spectrum. Figure 2(c) shows the combined normalized scattering spectrum of the sample with a plasmonic resonance at 774 nm. It is important to note that there is no plasmonic resonance observed in the fundamental region as well as the THG region (within the limits of our detection system).

Figure 3(a) shows the schematic of the nonlinear measurement setup and a schematic of the sample at top left. A 532 nm pump beam of 10 Hz repetition rate and 22 ps pulse width (Ekspla PL2241A) was used to generate a tunable p-polarized beam of 1200–1850 nm through a travelling wave parametric optical generator (Ekspla PG501). A longpass filter was used to remove the pump beam. A 10 nm gold substrate was used to split the beam to two portions, 40% of the beam was directed into a laser energy meter (Field MaxII-Top, Coherent) and 60% was focused onto the sample (the accurate percentage of the transmitted and reflected beam was measured for each wavelength separately). The source beam was aligned off-center of a 50 × microscope objective (0.85 NA, Melles Griot), focusing onto the sample, with the angle of incidence covering 45–58°. The spot size was estimated to be 30 ± 8 μm^2; therefore, there were approximately 9 ± 3 nanoparticles on average measured at a time. The scattered beam was directed to the same visible and near-IR spectrometers that used in the linear measurement. While it was possible to observe SHG, three photon photoluminescence and THG (as shown in Fig. 3(b)), at each wavelength and for each location on the sample, the setup was adjusted to maximize the THG signal (also shown in Fig. 3(b)). Optimizing the setup was done by adjusting the distance of the microscope objective from the sample and using the near-IR and visible spectrometers. The energy of the incident beam was set to be between 14 and 35 µJ per pulse at the sample spot, depending on the strength of the THG signal. In setting the energy of the incident beam for each wavelength, special care was taken to avoid damaging the sample. The fundamental signals were collected at the near-IR spectrometer with 500 ms acquisition time, averaged 5 times (shown in Fig. 3(c)). The corresponding THG signals were collected on the visible spectrometer CCD, with the same adjustment. Figure 3(d) shows the power-law dependence

#242926 Received 16 Jun 2015; revised 31 Aug 2015; accepted 8 Sep 2015; published 15 Sep 2015
(C) 2015 OSA

of THG signal characterized for one spot on the sample with varying the incident powers and noting the changes in the THG, giving a slope of 3.2 ± 0.2 on a log-log plot, which is close to the expected value of 3 for THG.

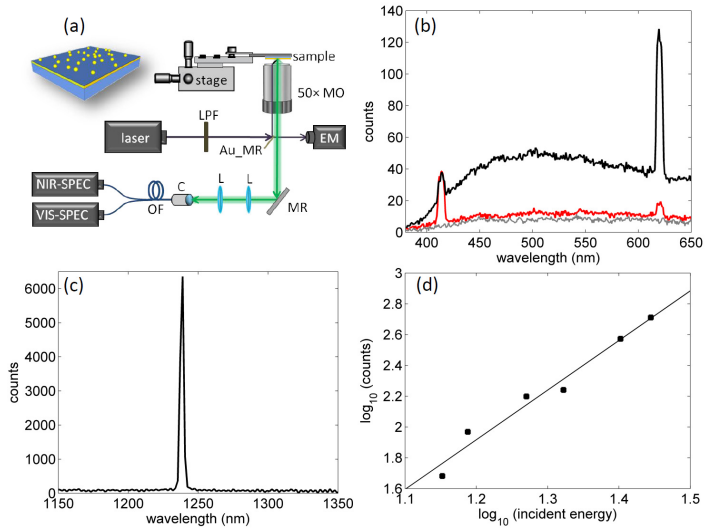

Fig. 3. (a) A schematic of the nonlinear measurement setup where LPF is longpass filter, Au-MR is 10 nm Au substrate used as beam splitter, MO is microscope objective, EM is energy meter, MR is mirror, L is lens, C is collimator, OF is optical fiber, NIR-SPEC is near-IR spectrometer, and VIS-SPEC is visible spectrometer. Top left is a schematic of the sample, gold nanoparticles-over-gold film separated by a SAM. (b) Spectrum of nonlinear conversion showing with black curve THG, SHG and a broad three photon photoluminescence. Red curve shows optimized THG where THG signal is maximized by adjusting the focus. Grey curve shows signal from the film only with no clear THG but some three photon photoluminescence. Background counts are subtracted from the curves. (c) Spectrum of the fundamental beam that was the source of the nonlinear spectrum shown in (b) after maximizing the THG signals (red curve). (d) The power-law dependence of THG signal, measured on one spot for incident energy varying between 14 μJ per pulse and 28 μJ per pulse, gives a slope of 3.2 ± 0.2 on a log-log plot.

3. Results and discussion

Figure 4(a) shows the THG response as a function of wavelength. The counts per pulse have been normalized to the pulse energy cubed and calibrated using a black-body source of known temperature (LS1, Ocean Optics). For each wavelength, the standard deviation indicated by the error bar was obtained from measurements at several different locations on two separate samples. The THG response of both samples showed the same response as a function of wavelength. The greater standard deviation around the peak is expected due to the third power dependence of THG on the local field intensity. The THG shows peaks in the range of 470 nm to 550 nm. There are also smaller peaks (at 413 nm, 433 nm and 600 nm), which may also contain contributions from the interband transitions. The average value of the largest peak is 35 × larger than the smallest value over the range. This is a considerable enhancement since we are probing the nearly instantaneous nonlinear response resulting in THG signal. However, the non-instantaneous nonlinear responses can result in three-four orders of magnitude enhancement in $\chi^{(3)}$ but not THG signal [29,44,45]. Also, it should be mentioned that nonlinear measurements of bare gold film, without nanoparticles, did not show THG signal, even for much higher incident energies. Using the nanoparticles-over-film system allows for picosecond excitation and efficient generation without damaging the sample since there is not broad area heating.

#242926 Received 16 Jun 2015; revised 31 Aug 2015; accepted 8 Sep 2015; published 15 Sep 2015

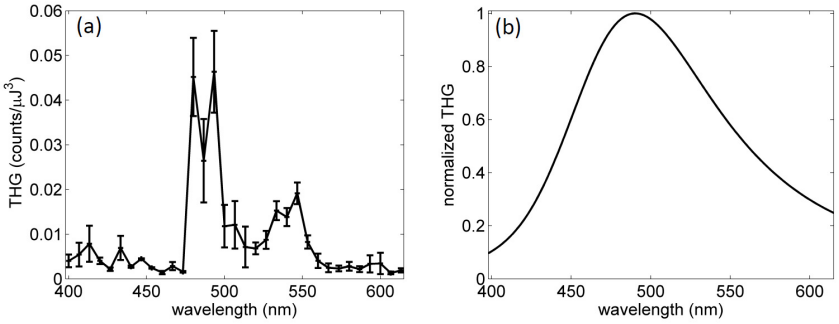

Fig. 4. (a) Normalized THG response as a function of wavelength. Counts per pulse have been normalized to the pulse energy cubed and calibrated using a black-body source of known temperature. The THG shows peaks in the range of 470 nm to 550 nm, which we attribute to the interband transition enhancements. For each wavelength, the standard deviation was obtained from measurements at different locations on two separate samples. (b) Normalized THG response calculated using a simple linear-polarization model for the third order susceptibility.

To understand this discrepancy, we applied a simple theory to model wavelength dependence $\chi^{(3)}$ of gold using the linear susceptibility $\chi^{(1)}$ to estimate the interband transition response (Ref. 21, Eq. (1).4.53):

$$\chi^{(3)}(\omega) = \frac{bm}{N^3 e^4}\left[\left(\chi^{(1)}(\omega)\right)^3 \chi^{(1)}(\omega_{\mathrm{THG}})\right] \tag{1}$$

where b is a parameter that characterize the strength of the nonlinearity, m is the electron mass, N is the electron density, and e is the electron charge. The fundamental wavelength ($\lambda = 2\pi c/\omega$) varies from 1200 nm to 1840 nm. We use an analytic model for the interband transition contributions to the linear response [30,50]:

$$\chi^{(1)}_{\mathrm{Au,interband}}(\lambda) = \frac{\mathrm{A}_1}{\lambda_1}\left(\frac{\exp\left(-i\frac{\pi}{4}\right)}{\left(\frac{1}{\lambda_1}-\frac{1}{\lambda}-\frac{i}{\gamma_1}\right)}+\frac{\exp\left(i\frac{\pi}{4}\right)}{\left(\frac{1}{\lambda_1}+\frac{1}{\lambda}+\frac{i}{\gamma_1}\right)}\right)+\frac{\mathrm{A}_2}{\lambda_2}\left(\frac{\exp(-i\frac{\pi}{4})}{\left(\frac{1}{\lambda_2}-\frac{1}{\lambda}-\frac{i}{\gamma_2}\right)}+\frac{\exp(i\frac{\pi}{4})}{\left(\frac{1}{\lambda_2}+\frac{1}{\lambda}+\frac{i}{\gamma_2}\right)}\right) \tag{2}$$

where $A_1 = 0.94$ and $A_2 = 1.36$ are the critical point amplitudes, $\lambda_1 = 468$ nm and $\lambda_2 = 331$ nm are the interband transition wavelengths, and $\gamma_1 = 2300$ nm and $\gamma_2 = 940$ nm are broadening factors (parameters taken from Ref. 30). It should be noted that the critical point amplitudes of this model provide a more accurate description of the asymmetric lineshape at the bandedge than the typical Lorentzian oscillator models used.

Relatively good agreement is seen between the peak location and relative amplitude of this simple model and the observed THG, without any additional fitting parameters, as shown in Fig. 4(b). This supports the claim that the enhancements maybe attributed to the interband transition in gold and that the response amplitude is governed by the electromagnetic transition dipole in that regime. It is interesting to note, however, that the experimental observations show more structure than the simple model predicts. For example, there is an abrupt reduction in THG in the range from 470 nm to 460 nm and an unexpected minimum around 520 nm. We have ensured that these are bona fide features of the sample and not related to the source or other absorptions in the setup. These features suggest that THG is sensitive to subtle variations in the interband transition strength and possibly dispersion of electron/hole scattering rates (e.g., hotter carriers may relax faster [51–54]). This is of obvious

#242926 Received 16 Jun 2015; revised 31 Aug 2015; accepted 8 Sep 2015; published 15 Sep 2015

interest for future comprehensive theory development, which is beyond the scope of this experimental work.

The observed response is of practical interest for applications seeking to use THG of plasmonic particles as a local probe, for example, in deep-tissue imaging where the long fundamental wavelength can penetrate deeper without scattering. In particular, this work shows that while enhancement is found at standard telecom wavelengths of 1550 nm where inexpensive femtosecond sources are abundant, the greatest enhancement would require excitation closer to 1500 nm. On the other hand, working at ~1640 nm may be preferred to avoid heating from water [55].

3. Conclusions

We investigated the wavelength dependence of THG from gold nanoparticles over a metal film with a thin spacer gap, for the situation where the fundamental beam energy was approximately one third of the interband transition energy, i.e., the resonant case. We found that the THG is enhanced by an order of magnitude by the interband transition (as compared to the non-resonant case). This significant enhancement for gold is of interest for applications where fiber-optic technology can be coupled to nonlinear plasmonics using gold. This is not limited to the system studied here of NPs over an ultraflat film; for example, this may be applied to deep tissue imaging using isolated metal nanoparticles as local probes [26,27]. For such applications, optimization of the plasmonic resonances should be used to maximize the signal, which can be both at the fundamental and third harmonic wavelengths. For example, there are nanorods with the longitudinal resonance around 1500 nm and the transverse resonance around 500 nm [56].

Acknowledgments

The authors acknowledge funding from the NSERC Discovery Grants program, and thank Sandra Roy and Dr. Paul Covert for their support in using the laser setup.

#242926 Received 16 Jun 2015; revised 31 Aug 2015; accepted 8 Sep 2015; published 15 Sep 2015
(C) 2015 OSA